MNRAS **000**, 1–15 (2016) Preprint 29 March 2016 Compiled using MNRAS LATEX style file v3.0

Supernovae and their host galaxies – IV. The distribution of supernovae relative to spiral arms

L. S. Aramyan,[1⋆] A. A. Hakobyan,[1†] A. R. Petrosian,[1] V. de Lapparent,[2] E. Bertin,[2] G. A. Mamon,[2] D. Kunth,[2] T. A. Nazaryan,[1] V. Adibekyan[3] and M. Turatto[4]

[1] *Byurakan Astrophysical Observatory, 0213 Byurakan, Aragatsotn province, Armenia*
[2] *Institut d'Astrophysique de Paris (UMR 7095: CNRS & UPMC), 98bis Bd Arago, F-75014 Paris, France*
[3] *Instituto de Astrofísica e Ciência do Espaço, Universidade do Porto, CAUP, Rua das Estrelas, P-4150-762 Porto, Portugal*
[4] *INAF – Osservatorio Astronomico di Padova, Vicolo dell'Osservatorio 5, I-35122 Padova, Italy*

arXiv:1603.08096v1 [astro-ph.GA] 26 Mar 2016

Accepted ... . Received ... ; in original form ...

ABSTRACT

Using a sample of 215 supernovae (SNe), we analyze their positions relative to the spiral arms of their host galaxies, distinguishing grand-design (GD) spirals from non-GD (NGD) galaxies. We find that: (1) in GD galaxies, an offset exists between the positions of Ia and core-collapse (CC) SNe relative to the peaks of arms, while in NGD galaxies the positions show no such shifts; (2) in GD galaxies, the positions of CC SNe relative to the peaks of arms are correlated with the radial distance from the galaxy nucleus. Inside (outside) the corotation radius, CC SNe are found closer to the inner (outer) edge. No such correlation is observed for SNe in NGD galaxies nor for SNe Ia in either galaxy class; (3) in GD galaxies, SNe Ibc occur closer to the leading edges of the arms than do SNe II, while in NGD galaxies they are more concentrated towards the peaks of arms. In both samples of hosts, the distributions of SNe Ia relative to the arms have broader wings. These observations suggest that shocks in spiral arms of GD galaxies trigger star formation in the leading edges of arms affecting the distributions of CC SNe (known to have short-lived progenitors). The closer locations of SNe Ibc vs. SNe II relative to the leading edges of the arms supports the belief that SNe Ibc have more massive progenitors. SNe Ia having less massive and older progenitors, have more time to drift away from the leading edge of the spiral arms.

Key words: supernovae: general – galaxies: spiral – galaxies: kinematics and dynamics – galaxies: stellar content – galaxies: structure.

1 INTRODUCTION

Many studies have been performed to find the links between different types of supernovae (SNe) and stellar populations of host galaxies (e.g. Navasardyan et al. 2001; Anderson & James 2009; Hakobyan et al. 2009; Habergham, James & Anderson 2012; Kelly & Kirshner 2012; Georgy et al. 2012; Nazaryan et al. 2013; Anderson et al. 2015), and estimate the possible ages of SN progenitors (e.g. Anderson et al. 2012; Kuncarayakti et al. 2013a,b; Crowther 2013). Studies of the spatial distribution of SNe in host galaxies give further insights on the nature of their progenitors. In particular, the relations between distributions of SNe and star formation in spiral arms are important in this context (e.g. Bartunov, Tsvetkov & Filimonova 1994; McMillan & Ciardullo 1996; Petrosian et al. 2005; Mikhailova, Bartunov & Tsvetkov 2007).

It is well known that star forming regions in spiral discs are generally concentrated in spiral arms (e.g. Seigar & James 2002). There are a variety of known structures of spiral galaxies, with different numbers and shapes of their arms (for recent review see Buta 2013). According to their spiral features, spiral galaxies are divided into three main types: 1) grand-design (GD) spirals with typically two arms; 2) flocculent spirals with many short arms; and 3) multi-armed spirals with several long spirals. Spiral arms in GD galaxies are thought to be density waves and may in fact represent quasi-steady wave modes (e.g. Bertin et al. 1989; Zhang 1996,

⋆ E-mail: aramyan@bao.sci.am
† E-mail: hakobyan@bao.sci.am

© 2016 The Authors

1998, 1999). However, there is also another interpretation, largely based on simulations, in which such arms are short-lived and recurrent structures (see review by Sellwood 2013). GD galaxies are usually associated with stellar bars (e.g. Sanders & Huntley 1976; Elmegreen & Elmegreen 1989; Ann & Lee 2013), or density waves caused by the tidal field of a nearby neighbor (e.g. Toomre & Toomre 1972; Kormendy & Norman 1979; Kendall, Kennicutt & Clarke 2011; Casteels et al. 2013). In contrast to GD spiral galaxies, flocculent and multi-armed spiral galaxies are likely formed from gravitational instabilities, or are sheared star formation regions (e.g. Seiden & Gerola 1982; Elmegreen, Elmegreen & Leitner 2003).

The distribution of stellar ages in spiral arms have been studied in GD galaxies. Investigating the dynamics of spiral galaxies, Roberts (1969) proposed that the piled up gas in a spiral arm experiences a strong shock that triggers star formation. He suggested that in the case of trailing spiral arms, young stars and HII regions inside the corotation radius are located in the inner edges of observable arms, and in the case of leading spirals they occur in the outer edges. Many studies were performed to find the predicted offsets between tracers of star formation (e.g. Vogel et al. 1988; Garcia-Burillo, Guelin & Cernicharo 1993) using eye-determination of the offsets, which could potentially affect the results. Applying a numerical method on 14 nearby disc galaxies, Tamburro et al. (2008) found that the radial dependence of the azimuthal offset between the HI and 24 μm emission is in agreement with the prediction of Roberts (1969). However, using the same method for another sample, Foyle et al. (2011) found no systematic ordering of angular offsets.

The study of different types of SNe as tracers of star formation caused by density waves and their distributions relative to spiral arms can help to better constrain the nature of SN progenitors. Types Ib, Ic, and II SNe, collectively called core-collapse (CC) SNe, are considered to be a result of gravitational collapse of young massive stellar cores in the final stage of the stellar evolution with initial masses $\geqslant 8\ M_{\odot}$. Moreover, CC SNe are well associated with star-forming sites (e.g. van Dyk et al. 1996; Tsvetkov et al. 2001; James & Anderson 2006; Anderson & James 2008; Anderson et al. 2012). SNe Ia are thought to originate from a thermonuclear explosion of C/O white dwarfs (e.g. Maoz & Mannucci 2012). The rate of SNe Ia in spiral galaxies suggests that a significant fraction of their progenitors belongs to the stellar population with intermediate ages and they can be considered as weak tracers of star formation (e.g. Cappellaro, Evans & Turatto 1999; Mannucci et al. 2005; Li et al. 2011; Hakobyan et al. 2011).

In the pioneering study of Moore (1973), the locations of 19 SNe in host galaxies were investigated. He found that over half of the SNe occur at the innermost edge of a spiral arm, and estimated that their lifetimes are less than five million years with masses greater than 35 $M_{\odot}$. Maza & van den Bergh (1976) measured the positions of 84 SNe relative to the spiral arms and found that the locations of SNe II are more concentrated relative to the arms than are the locations of SNe I (at that time SN types Ia, Ib, and Ic were not considered separately). Using a larger sample, Bartunov et al. (1994) studied the distribution of SNe Ia, Ib/c, and II relative to spiral arms and found that all SNe are distributed closer to the spiral arms comparing with random distribution in discs. McMillan & Ciardullo (1996) and Petrosian et al. (2005) found that CC SNe are more tightly concentrated to the arms than Ia. Finally, Mikhailova et al. (2007) found that SNe Ibc[1] are concentrated to the inner edges of the spiral arms. They noted that there is a difference between the distribution of Ibc and II SNe, and conclude that the progenitors of Ibc SNe are younger.

These studies used different samples of SNe, various methods of analysis and inhomogeneous data of SNe and their host galaxies. In particular, the spiral arms were traced by images of different quality, which is caused by various distances of the objects, exposure times, filters, etc. In addition, widths, shapes, and edges of spiral arms usually were determined visually, which also could affect the results.

In our first paper of this series (Hakobyan et al. 2012, hereafter Paper I) we have reported the creation of a large and well-defined data base that combines extensive new measurements and a literature search of 3876 SNe and their 3679 host galaxies located in the sky area covered by the SDSS Data Release 8 (DR8). This data base is much larger than all previous ones, and provides a homogenous set of global parameters of SN hosts, including morphological classifications and measures of activity classes of nuclei. In addition, we have analysed and discussed many selection effects and biases, which usually affect the studies of SNe. In the second paper (Hakobyan et al. 2014, hereafter Paper II), we have analysed the number ratios of different SN types in spirals with various morphologies and in barred and unbarred galaxies, different levels of morphological disturbance, and activity classes of nucleus. We proposed that the underlying mechanisms shaping the number ratios of SN types could be interpreted within the framework of interaction-induced star formation, in addition to the known relations between morphologies and stellar populations. In the third paper (Hakobyan et al. 2016, hereafter Paper III), we have presented an analysis of the impact of bars and bulges on the radial distributions of SNe in the stellar discs of S0–Sm host galaxies. We suggested that the additional mechanism shaping the distributions of Type Ia and CC SNe can be explained within the framework of substantial suppression of massive star formation in the radial range swept by strong bars, particularly in early-type spirals. We refer the reader to Papers I, II and III for more details.

In this fourth paper of the series, we investigate the distribution of different types of SNe relative to spiral arms taking into account the intrinsic properties of arms in order to find links between the distributions of the various SN types and arm's stellar populations. Moreover, considering possible differences of the distributions of various stellar populations in GD and multi-armed/flocculent spirals (e.g. Dobbs & Pringle 2010; Sánchez-Gil et al. 2011), we investigate the distribution of SNe in these subsamples of host galaxies.

The outline of this paper is as follows: Section 2 describes the sample. In Section 3, we provide a description of the spiral arm classification and extraction from the images, and the arm tracing method in the vicinity

[1] By SN Ibc, we denote stripped-envelope SNe of Type Ib, Ic, and mixed Ib/c whose specific subclassification is uncertain.

of the SN. We present our results in Section 4 and discuss them in Section 5. Our conclusions are summarized in Section 6. Throughout this paper, we adopt a flat cosmological model with $\Omega_{\rm m} = 0.27$, $\Omega_\Lambda = 0.73$ and a Hubble constant $H_0 = 73\,{\rm km\,s^{-1}\,Mpc^{-1}}$ (Spergel et al. 2007), both to conform with the values used in our data base (Paper I).

2 SAMPLE SELECTION

The sample of this study is drawn from the catalog of Paper I,[2] which contains 3876 SNe (72 SNe I, 1990 SNe Ia, 234 SNe Ibc, 870 SNe II, and 710 unclassified SNe) from the area covered by the SDSS DR8 and homogeneously measured parameters of their host galaxies. Note that for SNe II it includes also subtypes IIP, IIL, IIn, and IIb. The last SN included in the sample of Paper I is SN 2011bl, discovered on 2011 April 5.

The analysis of the distribution of SNe relative to spiral arms requires a well-defined sample and high angular resolution images of the SNe hosts. We selected our sample of SNe and their hosts according to the following criteria:

- SNe with available spectroscopic classification;
- SNe with available measurement of position[3];
- SNe located outside the circumnuclear region (we set a lower limit of 15 per cent of the host galaxy angular radius $R_{\rm SN}/R_{25} > 0.15$)[4], as well as outside any bar, interarm HII region[5] or overlapping region of two spiral arms;
- host galaxies with Sa–Sd morphological types;
- host galaxies without a strong morphological disturbance (excluding interacting, merging and post-merging classes of Paper II);
- host galaxies with angular size $D_{25} \geqslant 40''$ (to better distinguish the spiral arms);
- host galaxies with inclination $i \leqslant 40^\circ$ (to minimize absorption and projection effects);
- host galaxies whose surface brightness are not strongly contaminated by foreground Milky Way stars[6].

After applying these restrictions, the final sample of our study consists of 215 SNe in 187 host galaxies. The distribution of the different types of SNe according to the host galaxies morphological types is given in Table 1.

Table 1. Distribution of SN types according to the morphological classification of their host galaxies

	Sa	Sab	Sb	Sbc	Sc	Scd	Sd	All
Ia	5	4	8	16	25	5	2	65
Ibc	2	1	1	9	9	2	1	25
II	0	1	19	21	58	13	13	125
All	7	6	28	46	92	20	16	215

SNe Ib and Ic are not considered separately for lack of sufficient numbers (only 4 SNe Ib). Among SNe II, 6 are of Type IIb and 18 are of Type IIn.

3 DATA REDUCTION

In our study, the background subtracted and photometrically calibrated g-band images from the SDSS DR8 were used: among the SDSS channels with good signal-to-noise ratio (g, r, i), the arm-interarm contrast is the highest in the g-band, as it traces the young stellar populations in the spiral arms. These images were further analyzed to distinguish the spiral arms from the interarm regions. The whole reduction process is given below.

3.1 Determination of spiral arm classes

The spiral arm classes of all 187 host galaxies were determined visually from the g-band SDSS images, following the spiral arm classification of Elmegreen & Elmegreen (1987), who gave a numerical designation of arms according to flocculence and degree of chaos. The galaxies with arm class 12 contain only two long and symmetric arms dominating the optical disc, and the ones with class 9 have two inner symmetric arms, and multiple long outer arms. In all other cases the arms are fragmented (classes between 1 and 4), feathery/irregular (classes between 5 and 7) or tightly warped/ring-like (class 8). Classes 10 and 11 were previously denoted to bars and companions and are no longer used. Then the galaxies were assigned as GD (classes 9 and 12) or non-GD (NGD, all classes except 9 and 12).

According to Elmegreen & Elmegreen (1987), the most common mis-classifications of arm classes are from 2 or 3 to 4 or 5 (or vice versa) and from 9 to 12 (or vice versa). Because we separate the host galaxies arm classes into two broad subsamples GD and NGD, the possible misclassification of GD into NGD (or vice versa) is negligible.

In order to test our classification, the whole sample of host galaxies was classified twice by two different coauthors. By comparing these two classifications, we determined that our classification was 97 per cent reliable.

3.2 Spiral arm structures

Using the version 2.18.4 of SExtractor software (Bertin & Arnouts 1996), we carried out a procedure to isolate the spiral structure of the galaxies. We first fitted all g-band SDSS images of the host galaxies in the sample with bulge+disc models ($r^{1/4}$ bulge and exponential disc profiles are used for all galaxies).

The modeled bulge+disc was then subtracted from each original image. In the following, we describe how we use the residual image for determining the location of the spiral arms and their radial profile relative to the position of the SN. Fig. 1 illustrates the procedure on two spiral galaxies.

[2] Parameters of several SNe and their host galaxies were revised in Aramyan et al. (2013).
[3] The SN position is usually provided by the SN catalogues via its offset from the host galaxy nucleus, or equatorial coordinates.
[4] R_{25} is the host galaxy g-band 25th magnitude isophotal radius $R_{25} = D_{25}/2$.
[5] In bulge+disc subtracted images SNe 2001ed (Ia) and 1961I (II) are located on interarm HII regions and thus are excluded from our sample.
[6] We selected only host galaxies for which at least two of inner edge, outer edge, and the arm peak were determined.

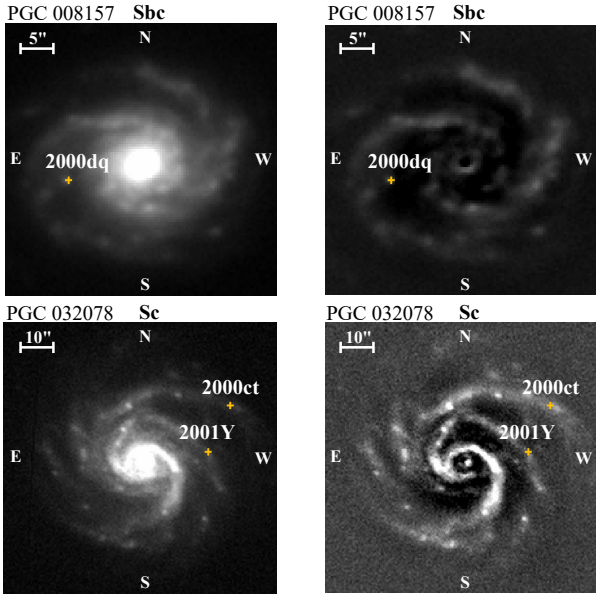

Figure 1. Examples of the original (left) SDSS *g*-band and bulge+disc subtracted (right) images of SNe host galaxies. The PGC object identifiers and morphological types are listed at the top. The SN names and positions (marked by a cross sign) are also shown. In all images, north is up and east to the left.

3.3 Position of SN with respect to spiral arm

To avoid effects due to different distances of the host galaxies, the image of the host galaxy is smoothed with a Gaussian filter with $\sigma = 0.25$ pixel $\times\, 100/D$, where D is the comoving distance of the galaxy in Mpc. Because the exponential fits of the discs use light from both the arm and interarm regions, the values of pixels in the interarm regions of the residual images are negative. These are replaced with a null value, and a zero threshold defines the inner and outer borders of the spiral arms.

To study the distribution of SNe with respect to spiral arms, at first the closest spiral arm structure to the SN is defined (for *interarm* SN we define the closest spiral arm as the one with the closest edge). The closest segment of spiral arm to SN position is fixed along the radial line passing through the galaxy nucleus and SN location (e.g. upper panel of Fig. 2). The radial light profile is obtained using the SAO DS9 analysis tool with the *linear region* option. The coordinates of the nucleus and the isophotal radius R_{25} of the host galaxies are those provided in the data base of Paper I. Accordingly, arm profiles are constructed (bottom panel of Fig. 2). Four representative arm profiles of GD spirals and four arm profiles of NGD spirals are given respectively in the left- and right-hand panels of Fig. 3.

We define *arm* and *interarm* SNe, those that respectively lie inside the arm borders or in the interarm region, respectively.

In the cases when the profile is contaminated by star(s) or by the SN (when the SN is still visible in the SDSS image, e.g. SN 2000dq in Figs. 1 and 3), we fit the contaminant with a Gaussian profile and subsequently subtract it from the global profile. In the cases when the edges of several spiral arms overlap, we fit the profile with a multi-Gaussian

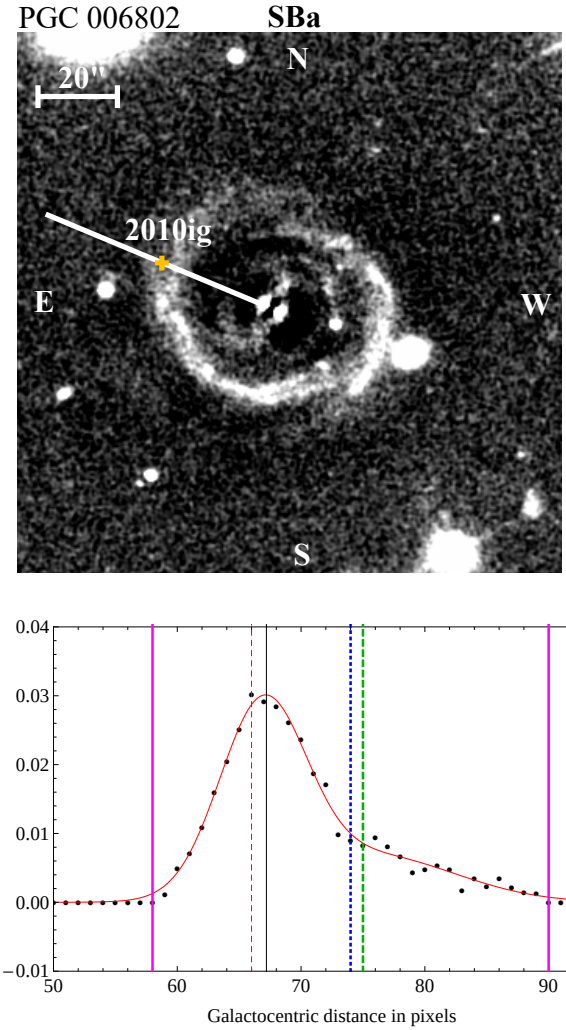

Figure 2. *Upper panel:* residual SDSS *g*-band image of the host galaxy of SN 2010ig, after subtracting the best fit bulge+disc components. The PGC object identifier and morphological type are listed at the top of the figure (north is up and east to the left). The SN name, position (marked by a cross sign), and SN radial line are also shown. *Bottom panel:* brightness profile along the SN radial line and its fit (thin red line) with a multi-peak Gaussian. The vertical lines represent the position of the SN (green thick dashed), the edges (thick magenta), middle (blue thick dotted) and brightest pixel (thin dashed red), and peak of Gaussian fit (thin black) of the spiral arm.

function (the number of components equals the number of visible spiral arms). We also apply a multi-Gaussian when the brightest pixel is shifted from the middle of arm borders by more than 10 per cent of the arm width, or when the profile of the arm shows a multi-peak structure.

3.4 Normalized distances along arm profiles

To study the SNe distributions relative to spiral arms, two different approaches for the normalization of the distances

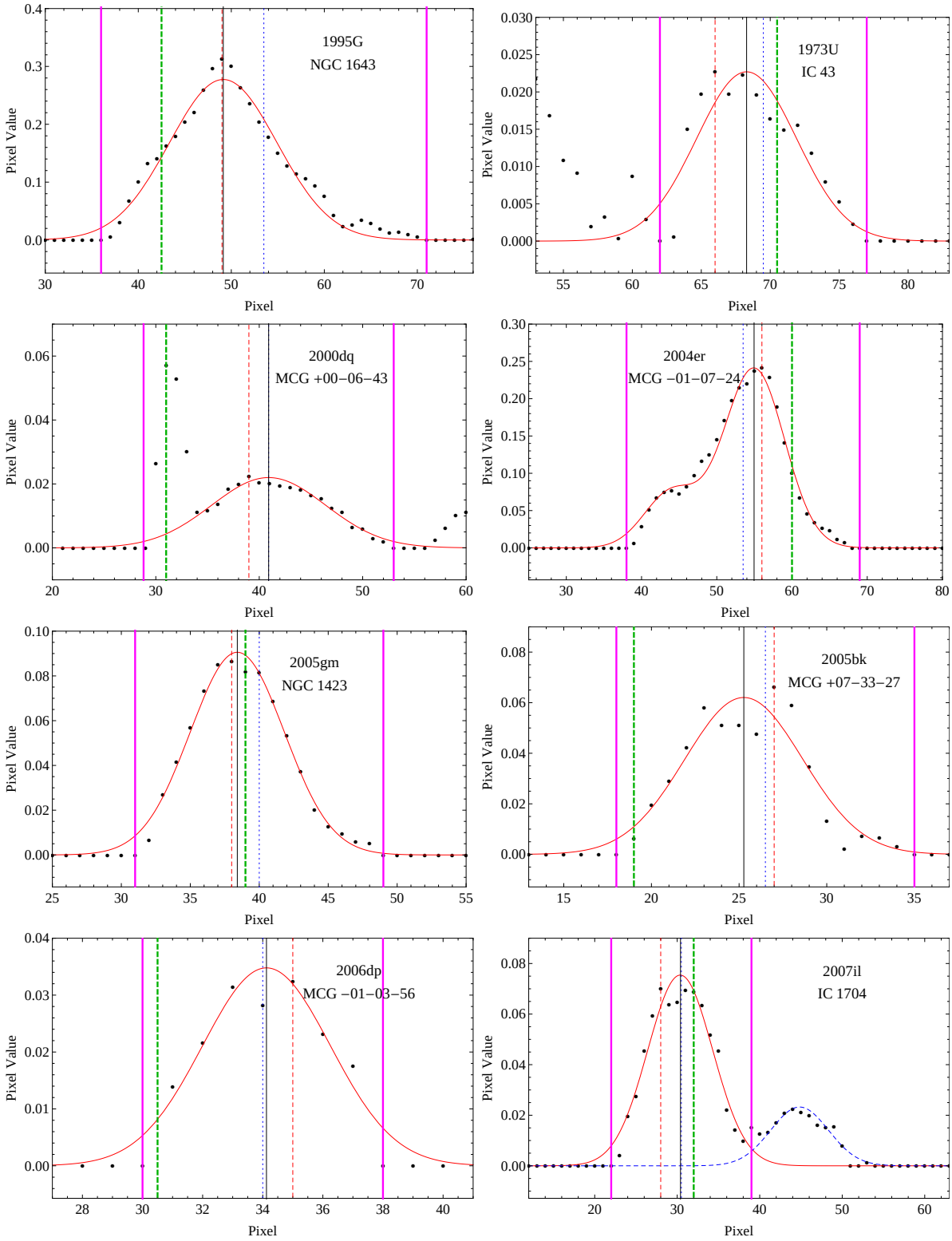

Figure 3. Four representative spiral arm intensity profiles for GD (*left*) and NGD (*right*) host galaxies. The SN positions, inner and outer edges, middles, as well the peaks and brightest pixels of spiral arms are shown with vertical lines, similar to Fig. 2. For SN 2007il, the best-fit profile of the contamination of the neighbor arm is shown as the dashed blue curve.

are applied. In the first approach, the distance[7] $d_{\rm SN}$ of an SN from the inner edge (at galactocentric radius $r = r_-$) of the spiral arm is normalized to the width W, defined as the distance between inner and outer edge (at galactocentric radius r_+) of the arm (e.g. Maza & van den Bergh 1976; Bartunov et al. 1994; Mikhailova et al. 2007):

$$d_1 = \frac{d_{\rm SN}}{W} = \frac{r_{\rm SN} - r_-}{r_+ - r_-} \ , \qquad (1)$$

where $W = r_+ - r_-$ is the width of the arm along the radius vector passing through the galaxy nucleus, as well as r_- and r_+ are the radial distances of inner and outer edges, respectively. It is important to note that due to the orbital motion of disc and spiral arms, the $r_{\rm SN} - r_-$ distance depends on the pitch angle of spiral arm, that can vary from galaxy to galaxy. However, the same dependence is true also for the arm width ($r_+ - r_-$), determined through the same radial direction. Therefore, the normalized distance has the advantage of being independent from the pitch angle of the considered segment of spiral arm.[8] According to this definition, *interarm* SNe close to the inner edge of the spiral arm have $d_1 < 0$, while *interarm* SNe closer to the outer edge have $d_1 > 1$.

We test whether the location of the peak of the best-fit multi-Gaussian changes according to the choice of the threshold value defining the inner and outer borders of the spiral arms. To this end, 10 arm profiles were randomly selected and for each 12 different thresholds were applied. These thresholds were uniformly distributed between 2/3 of the peak value and $1.5\,\sigma$ above the mean interarm value. For each threshold, we fit the arm profiles and determine the positions of the peaks. The test shows that the standard deviations of the distributions of the positions of arm peaks are about $0.02 - 0.03$ of the widths of arms.

Then, we pay attention to the distributions of g-band Gaussian peaks and brightest points in the arm profiles. Fig. 4 shows that the normalized distribution of both the brightest points and the peaks of the profiles are generally located closer to the inner edge than to the outer edge of the spiral arms. In other words, the arm profiles tend to be positively skewed.

In order to check the normality, we compare the distributions of peaks and brightest points in spiral arms with the Gaussian functions with fixed $\mu = 0.5$ (the mean of the distributions) and free μ, respectively. For this purpose we perform a maximum likelihood estimation to find the standard deviations and μ (for the second case) of the Gaussian. We then compare the distribution of $(r_{\rm peak} - r_-)/(r_+ - r_-)$ distances with the best fit functions. To examine the significance of the differences between the distributions in different samples (or between the sample and a best fit function), we employ the Kolmogorov-Smirnov (KS) and Anderson-Darling (AD) tests[9]. The corresponding KS and AD probabilities, $P^{\rm KS}_{\mu=1/2}$ and $P^{\rm AD}_{\mu=1/2}$, are given in Cols. 3 and 4, as well as $P^{\rm KS}_{\rm free-\mu}$ and $P^{\rm AD}_{\rm free-\mu}$ which are given in Cols. 5 and 6 of Table 2. Table 2 shows that both distributions are Gaussians that are significantly shifted from the middle of spiral arms towards the inner edges.

Table 2. The mean, standard deviation, $P_{\rm KS}$ and $P_{\rm AD}$ values of the normality tests of the $(r_{\rm peak} - r_-)/(r_+ - r_-)$ distances of arm peaks and brightest points (BP). The statistically significant differences are highlighted in bold.

	μ	σ	$P^{\rm KS}_{\mu=1/2}$	$P^{\rm AD}_{\mu=1/2}$	$P^{\rm KS}_{\rm free-\mu}$	$P^{\rm AD}_{\rm free-\mu}$
	(1)	(2)	(3)	(4)	(5)	(6)
Peak	0.47 ± 0.01	0.12 ± 0.01	**0.001**	**0.001**	0.803	0.884
BP	0.47 ± 0.01	0.16 ± 0.01	**0.003**	**0.005**	0.329	0.321

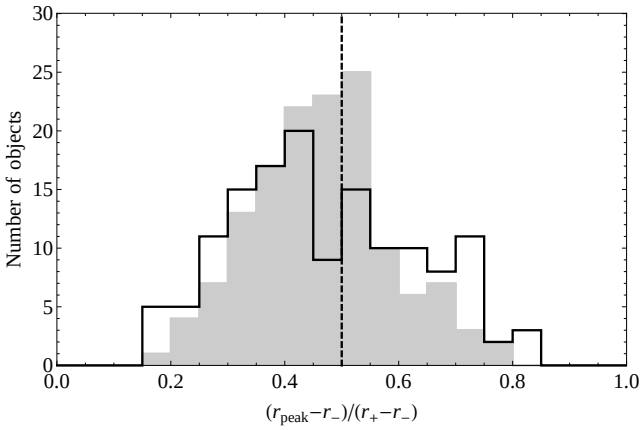

Figure 4. Distribution of the brightest pixels along spiral arms (open histogram) and peaks of Gaussian fits (shaded histogram) in the g-band images. The abscissa is zero and 1 at the inner and outer edges of the spiral arms, respectively. The cases when at least one of the edges is contaminated and not well-determined, are excluded from the histogram. The dashed line shows the middle of the arm.

It is important to note that the brightest points of the arm profiles are often associated with local HII regions and do not represent the general distributions of the g-band light profiles of the spiral arms. We therefore design a second normalization using either the distance between the peak of the spiral arm and its inner edge ($W_- = r_{\rm peak} - r_-$), or that between the peak and the outer edge ($W_+ = r_+ - r_{\rm peak}$), depending on whether the SN is located between the host galaxy nucleus and the peak of the spiral arm or outside this region (labeled $\rm SN_{in}$ and $\rm SN_{out}$ respectively in Fig. 5). The new normalized distance is then

$$d_2 = \frac{d_\pm}{W_\pm} = \frac{r_{\rm SN} - r_{\rm peak}}{|r_{{\rm sign}(r_{\rm SN} - r_{\rm peak})} - r_{\rm peak}|} \ , \qquad (2)$$

where

$$r_{\rm sign}(r_{\rm SN} - r_{\rm peak}) = \begin{cases} - & \text{for } r_{\rm SN} < r_{\rm peak} \ , \\ + & \text{for } r_{\rm SN} > r_{\rm peak} \ . \end{cases}$$

It is clear that, if we normalize the distances of SNe relative to spiral arms to the widths of arms, the distribution of normalized distances will be systematically shifted and enhanced to the inner part of spiral arms with respect to

[7] For all radial distance measurements, we used the deprojection method described in Hakobyan et al. (2009).
[8] It is worth mentioning that we consider only the orbital motion of SN progenitors, neglecting the possible radial migration. In Sect. 5, we discuss in more detail the motion of progenitors in the discs.
[9] The AD test is similar to the KS test, except that it is more sensitive to differences in the tails of distributions.

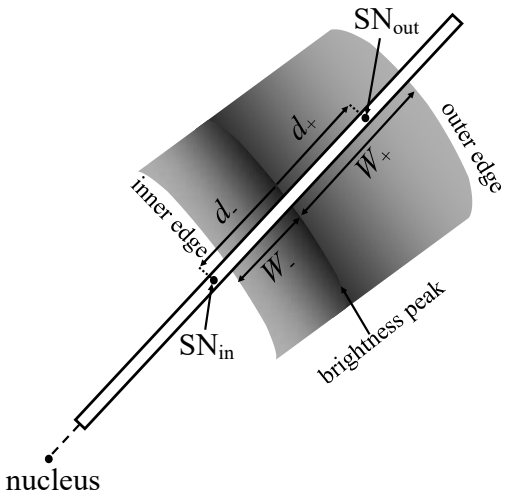

Figure 5. The scheme of normalization according to the location of the SN relative to spiral arm: when the SN is located in the inner part of the spiral arm (SN$_{in}$), and when the SN is located in the outer part of the arm (SN$_{out}$).

the second case. Most probably this effect is reflected in the results of Mikhailova et al. (2007), who found that the distribution of SNe Ibc is skewed towards the inner edges of arms.

We apply this normalization both when the SN is located inside the borders of the spiral arm (e.g. SN$_{out}$ in Fig. 5), and when the SN is located outside the borders of spiral arm (e.g. SN$_{in}$ in Fig. 5).

4 RESULTS

In this section, we present a detailed analysis of the distributions of SNe with different locations in GD and NGD spiral host galaxies. In particular, the distributions of SNe in the arm and interarm regions and their dependences on galactocentric distances are analyzed. Among the 215 SNe, 178 are arm SNe, while 37 are interarm SNe. The full list of arm and interarm SNe (Col. 1), their types (Col. 2), host galaxies names (Col. 3), morphological types (Col. 4), spiral arm classes (Col. 5), the SNe galactocentric distances (Col. 6), normalized distances d_1 (Col. 7) and d_2 (Col. 8) are given in Tables A1 and A2.

4.1 Distribution of SNe relative to spiral arms

The comparison of the distributions of different types of SNe located in spiral arms and interarm regions (Tables A1 and A2) shows that SNe Ibc are discovered only within spiral arms. The majority (88 ± 2 per cent) of SNe II also belongs

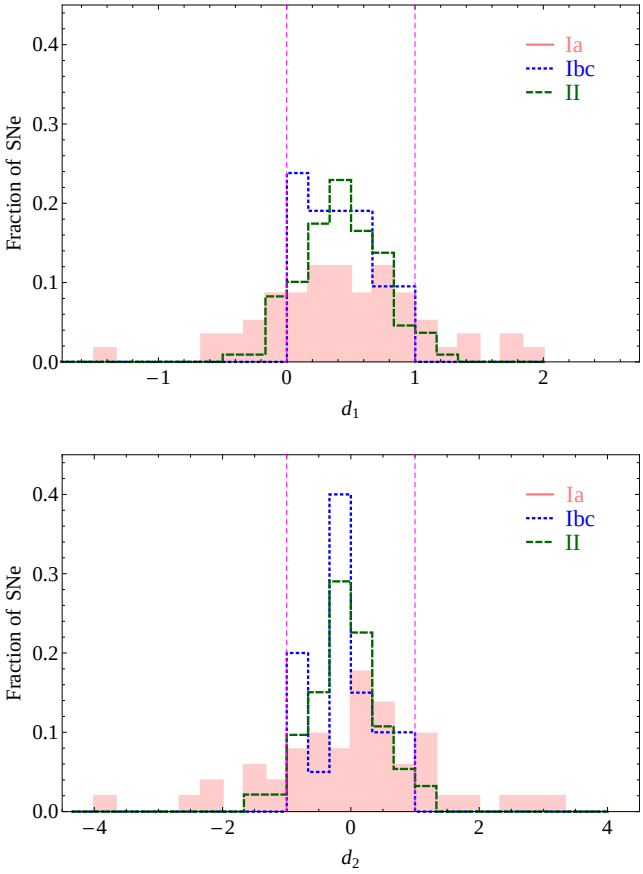

Figure 6. *Upper panel:* distributions of SN positions relative to the inner edge of the spiral arm normalized to the width of the arm (see eq. [1]). *Bottom panel:* distributions of SNe positions relative to the peaks of arms normalized to the inner/outer semi-widths (see eq. [2]). The data flagged by '*' symbols in Tables A1 and A2 are not considered in both panels. The filled red histograms represent SNe Ia, while the green dashed and blue dotted histograms represent SNe II and Ibc, respectively.

Table 3. The mean, standard deviation, P_{KS} and P_{AD} values of the normality tests of the d_1 distances. The statistically significant difference is highlighted in bold.

SN	$\langle d_1 \rangle$ (1)	σ (2)	$P^{KS}_{\mu=1/2}$ (3)	$P^{AD}_{\mu=1/2}$ (4)	$P^{KS}_{free-\mu}$ (5)	$P^{AD}_{free-\mu}$ (6)
Ia	0.46 ± 0.08	0.63 ± 0.07	0.967	0.931	1.000	0.997
Ibc	0.42 ± 0.05	0.26 ± 0.03	0.280	0.209	0.807	0.848
II	0.43 ± 0.03	0.32 ± 0.02	0.097	**0.039**	0.977	0.999

to spiral arms, while this percentage is only 66^{+3}_{-4} per cent for SNe Ia[10].

The distributions of *arm* and *interarm* SNe, with different normalizations discussed in Sect. 3.4, are presented in Fig. 6. The mean and standard deviation of the distributions of d_1 and d_2, with their bootstrapped (10^4 times) errors are given in Tables 3 and 4, respectively. The upper panel of Fig. 6 shows the distributions of SNe distances rel-

[10] The errors on fractions are calculated using the Bayesian approach of Cameron (2011).

Table 4. The mean, standard deviation, $P_{\rm KS}$ and $P_{\rm AD}$ values of the normality tests of the d_2 distances.

SN	$\langle d_2 \rangle$	σ	$P^{\rm KS}_{\mu=0}$	$P^{\rm AD}_{\mu=0}$	$P^{\rm KS}_{\rm free-\mu}$	$P^{\rm AD}_{\rm free-\mu}$
	(1)	(2)	(3)	(4)	(5)	(6)
Ia	0.01 ± 0.18	1.31 ± 0.16	0.815	0.733	0.850	0.743
Ibc	-0.07 ± 0.10	0.46 ± 0.06	0.443	0.615	0.818	0.823
II	-0.10 ± 0.06	0.56 ± 0.04	0.116	0.162	0.880	0.917

Table 5. Comparison of the distributions of the d_1 and d_2 distances between different types of SNe. The P-values of both KS and AD tests are given. The statistically significant differences are highlighted in bold.

Samples	d_1		d_2	
	$P_{\rm KS}$	$P_{\rm AD}$	$P_{\rm KS}$	$P_{\rm AD}$
Ia versus Ibc	0.109	0.073	0.137	0.054
Ibc versus II	0.835	0.780	0.921	0.829
II versus Ia	0.150	**0.013**	0.068	**0.005**

ative to the inner edges of spiral arms normalized to the width of the arm. This figure and Table 3 show that the distribution of SNe Ia ($\langle d_1 \rangle = 0.46 \pm 0.08$) has a symmetrical appearance to the middle of spiral arms. On the other hand, the distribution of SNe Ibc ($\langle d_1 \rangle = 0.42 \pm 0.05$) and SNe II ($\langle d_1 \rangle = 0.43 \pm 0.03$) are (respectively marginally and significantly) shifted towards the inner edges of arms. The excess of SNe Ibc toward inner edges of arms was also reported by Mikhailova et al. (2007). They pointed out that the distribution of SNe Ibc follows an exponential law relative to inner edges of spiral arms. However, they fitted with an exponential function the distribution of physical distances of SNe from inner edges, and reported a scale length of 1 kpc. The use of physical distances can significantly bias the results, because spiral arms display a variety of sizes and shapes.

We now check the consistency of SN locations relative to the spiral arms of their host galaxies, d_1, with the Gaussian function with mean $\mu = 0.5$. For this purpose we perform a maximum likelihood estimation to find the standard deviation of the Gaussian. We then compare the distribution of d_1 distances with the best fit function. The corresponding KS and AD probabilities, $P^{\rm KS}_{\mu=1/2}$ and $P^{\rm AD}_{\mu=1/2}$, are given in Cols. 3 and 4 of Table 3.

Then, we apply the same test, but without fixing the μ (the mean of the distributions). The $P^{\rm KS}_{\rm free-\mu}$ and $P^{\rm AD}_{\rm free-\mu}$ values (Cols. 5 and 6 in Table 3) show that the distributions of all types of SNe are consistent with a Gaussian function. However, $P^{\rm AD}_{\mu=1/2} = 0.039$ value (Col. 4 in Table 3) shows that the distribution of SNe II is not consistent with a symmetric distribution around the middle of the spiral arm. The inconsistency of the distribution of SNe Ibc with a symmetric one around the middle of the spiral arm is not significant ($P^{\rm KS}_{\mu=1/2} = 0.280$), probably because of small number statistics. The distribution of SNe Ia is not shifted ($P^{\rm KS}_{\mu=1/2} = 0.967$) with respect to the middle.

When comparing the distribution of d_1 distances of various SN types (Cols. 2 and 3 in Table 5), in contrast to the KS test ($P_{\rm KS} = 0.150$), the AD test shows significant difference between the distributions of SNe Ia and II ($P_{\rm AD} = 0.013$). The difference between the results of tests is due to the difference of distributions in the tails (see also Fig. 6). The difference between the distributions of SNe Ia and Ibc is not significant, probably because of the small number statistics. The distributions of SNe Ibc and II are not different as well.

We analyze next the relative positions of different SN types using the second normalization scheme presented in Sect. 3.4. These distributions are shown in the bottom panel of Fig. 6. The comparison of distributions of various types of SNe in the upper and bottom panels of Fig. 6 shows that with the second normalization, the maximum of SNe Ibc distribution is shifted from inner edges of spiral arms to their peaks (see also Table 4).

As for the first normalization scheme, we check the normality of the distribution of d_2 distances. The corresponding $P^{\rm KS}_{\mu=0}$, $P^{\rm AD}_{\mu=0}$, $P^{\rm KS}_{\rm free-\mu}$ and $P^{\rm AD}_{\rm free-\mu}$ values of KS and AD tests are given in Cols. 3, 4, 5 and 6 of the Table 4. These values show that, in contrast to d_1, the distributions of d_2 for all types of SNe are consistent with a Gaussian centred on the peaks of spiral arms. Therefore, the asymmetric distributions of SNe Ibc (obtained by Mikhailova et al. 2007) and II with respect to the middle of spiral arm are just an effect of first normalization scheme of SNe distances, which does not take into account the intrinsic structure of spiral arms.

The differences between the distributions presented in th bottom panel of Fig. 6 again are checked by KS and AD tests (Cols. 4 and 5 in Table 5). The tests show that there is a marginally significant difference (probably, because of small number statistics) between Ia and Ibc ($P_{\rm AD} = 0.054$) as well as a significant difference between Ia and II ($P_{\rm AD} = 0.005$) SNe distributions. The difference between the distributions of SNe Ibc and II is not statistically significant.

Analyzing the distribution parameters of d_2 for various SN types presented in Table 4, we note that the distributions of all types of SNe show a significant concentration around the peak of the spiral arm. The most concentrated is the distribution of SNe Ibc, then Types II and Ia. In addition, the distributions of d_2 distances for all SN types are Gaussian, without a significant shift from the peak of spiral arm profile. The observed large numbers of SNe Ia in interarm regions (Fig. 6) is attributed to their long-tailed distribution.

Thus, we show that the intrinsic structure of spiral arms play a crucial role shaping the distribution of CC SNe relative to arms. Therefore, in the remainder of this study we will present and discuss only the distributions of d_2 distances.

4.2 Distribution of SNe in GD and NGD hosts

The influence of density waves on the star formation in spiral galaxies has been one of the most debated problems, with contradicting observational results (for a recent review, see Dobbs & Baba 2014). Due to the short lifetimes of their progenitors (e.g. James & Anderson 2006; Smartt 2009; Anderson et al. 2012; Crowther 2013), different types of CC SNe, considered as tracers of star formation, can help to better understand the influence of density waves on star formation. Particularly, the comparative distribution of different types of SNe relative to spiral arms of the hosts can

Table 6. Distribution of SN types according to the host spiral arm classes.

	GD spirals	NGD spirals	All
Ia	29	36	65
Ibc	10	15	25
II	67	58	128
All	106	109	215

Table 7. The mean, standard deviation of d_2 distances, $P_{\rm KS}$ values of normality tests.

	$\langle d_2 \rangle$	σ	$P^{\rm KS}_{\mu=0}$	$P^{\rm KS}_{\rm free-\mu}$
Ia^{GD}	0.06 ± 0.29	1.37 ± 0.29	0.123	0.182
Ia^{NGD}	-0.03 ± 0.24	1.27 ± 0.19	0.972	0.972
CC^{GD}	-0.09 ± 0.06	0.51 ± 0.04	0.188	0.842
CC^{NGD}	-0.10 ± 0.08	0.59 ± 0.06	0.169	0.558

shed light on the nature of star formation in galaxies with different spiral structures.

In our sample of 187 SNe host galaxies, 89 are GD and 98 are NGD spirals. The distribution of SN types in GD and NGD spirals is presented in Table 6. Because of the small number of SNe Ibc in both samples (10 and 15 SNe Ibc in GD and NGD galaxies, respectively), they are merged with SNe II in the general class of CC SNe.

The distribution of Ia and CC SNe relative to the peaks of spiral arms in GD and NGD galaxies are presented in Fig. 7. The mean and standard deviation, with their bootstrapped (10^4 times) errors, as well the $P^{\rm KS}_{\mu=0}$ and $P^{\rm KS}_{\rm free-\mu}$ values of KS normality tests are given in Table 7. Here, the results of the AD test are not different from those of the KS test. The $P^{\rm KS}_{\mu=0}$ and $P^{\rm KS}_{\rm free-\mu}$ values show that the distributions of CC and Ia SNe in both types of host galaxies are consistent with Gaussian distributions centred on the peaks of spiral arms (Table 7).

The results of the comparison of the distributions of d_2 of Ia and CC SNe in GD and NGD galaxies is given in Table 8. The KS and AD tests show that, in both types of host galaxies, the d_2 radial positions of Type Ia and CC SNe within the spiral arms are significantly different. The KS probability that such differences could arise by chance are 0.012 (GD hosts) and 0.023 (NGD hosts).

Analyzing both panels of Fig. 7, we see that, in both types of host galaxies, CC SNe are concentrated towards the peaks of spiral arms. For SNe Ia, a concentration close to the peak of spiral arm in GD galaxies is observed, while not in NGD galaxies, which actually show a remarkable absence in the corresponding peak. Finally, comparison of CC (as well as Ia) SNe distributions in GD and NGD galaxies shows no significant difference (see Table 8).

It is interesting to note, that the distribution of CC SNe in NGD galaxies is more extended ($\sigma = 0.59 \pm 0.06$) than that in GD galaxies ($\sigma = 0.51 \pm 0.04$), although the difference is not statistically significant. There are more (16^{+3}_{-3} per cent) CC SNe (all of which are of Type II) in interarm regions of NGD than in interarm regions of GD galaxies (9^{+3}_{-2} per cent). From Table 7, we note that the sigmas (σ) of the distributions of SNe Ia in GD and NGD galaxies are consistent. The differences between the distributions of SNe Ia and CC SNe in both GD and NGD galaxies are attributed to the remarkably extended distributions of SNe Ia.

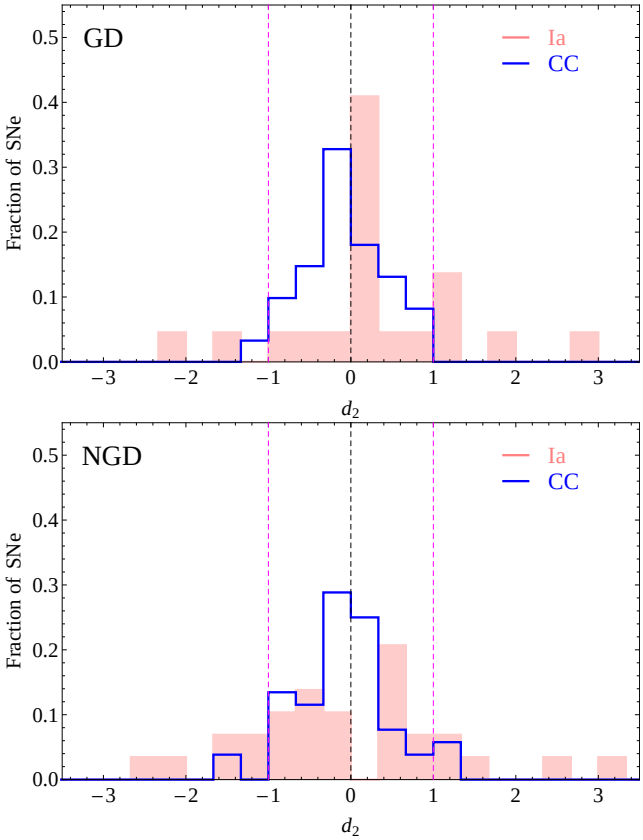

Figure 7. *Upper panel*: distributions of the locations of SNe Ia (filled histogram, 22 SNe) and CC (open histogram, 63 SNe) SNe relative to the peaks of spiral arms of GD galaxies. *Bottom panel*: distributions of the locations of SNe Ia (29 SNe) and CC SNe (53 SNe) SNe relative to the peaks of spiral arms of NGD galaxies. SNe with distance flags '*' and ':' are removed.

Table 8. Comparison of the distributions of the d_2 distances of various types of SNe in various arm classes of galaxies, using the KS and AD tests. The statistically significant differences are highlighted in bold.

Samples	$P_{\rm KS}$	$P_{\rm AD}$
Ia^{GD} versus CC^{GD}	**0.012**	**0.010**
Ia^{NGD} versus CC^{NGD}	**0.023**	**0.025**
Ia^{GD} versus Ia^{NGD}	0.231	0.461
CC^{GD} versus CC^{NGD}	0.981	0.847

4.3 Radial behaviour of SNe distributions in spiral arms

The spatial distribution of SNe in host galaxies provides strong constraints on the nature of SN progenitors as well establishes the relations with stellar population of the

galaxies. Various studies show that CC SNe are tightly connected to discs (e.g. Paper III) and spiral arms (e.g. van Dyk et al. 1996), which differs from the distribution of SNe Ia in the arms (e.g. McMillan & Ciardullo 1996). In addition, studying the radial distributions of the sample of SNe Ibc and II, several authors have found that the mean galactocentric distance of SNe Ibc is smaller than that of SNe II (e.g. van den Bergh 1997; Boissier & Prantzos 2009; Anderson & James 2009; Hakobyan et al. 2009; Paper III).

Therefore, we investigate the possible dependence of d_2 on the deprojected radii ($R_{\rm SN}$) of the SNe, normalized to the R_{25} of their hosts ($R_{\rm SN}/R_{25}$). Fig. 8 presents the radial trend for various SN types. Since we aim to investigate the possible influence of density waves on the distribution of SNe in spiral arms, here we consider only *arm* SNe, although, for better visualization, the interarm SNe are also shown in Fig. 8. In the full (GD+NGD) sample of hosts for both types of CC SNe, there is a positive correlation between d_2 and $R_{\rm SN}/R_{25}$ (see solid trendlines in the middle and bottom panels of Fig. 8). Both SNe Ibc and II at smaller radii are enhanced in the inner parts of spiral arms (before the peak of spiral arm), and at larger radii the enhancement is shifted to the outer parts (after the peak of spiral arm).

Interestingly, Figure 8 indicates that the trendlines of SNe Ibc and II cross the arm peak at approximately the same galactocentric distances. Noting that the corotation radii reported in Scarano & Lépine (2013), normalized to the R_{25} of each galaxy, obey $\langle r_{\rm cor}/R_{25}\rangle \approx 0.45 \pm 0.03$, we find that the trendlines of SNe Ibc and II cross the arm peak at roughly the location of the corotation radius.

To check the significance of the radial trends, we use the Spearman's rank correlation test. For the full sample of the hosts, the P-values of the hypothesis that there is no dependence between d_2 and $R_{\rm SN}/R_{25}$ are presented in Column 5 of Table 9. The number of SNe, a coefficient of the $d_2 = a\,(R_{\rm SN}/R_{25})+b$ linear interpolation between d_2 and $R_{\rm SN}/R_{25}$, and ρ parameter of Spearman's rank correlation test are given in Cols. 2, 3 and 4 of Table 9, respectively. Table 9 shows that the trends for both SNe Ibc and II in the full sample are significant.

To strengthen the results, we merge together SNe Ibc and SNe II into a CC SNe sample. We use the $\langle r_{\rm cor}/R_{25}\rangle$ demarcation radius to separate the samples of SNe into two radial bins. The KS and AD tests show that the difference of d_2 distributions of CC SNe in these radial bins is statistically significant ($P_{\rm KS} = 0.036$ and $P_{\rm AD} = 0.010$).

Summarizing the results for SNe Ibc and II in the full sample, we conclude that: (1) there are significant positive correlations between d_2 and $R_{\rm SN}/R_{25}$; (2) in most cases, the positions of CC SNe are inside (outside) the peak of the spiral arms for galactocentric radii smaller (larger) than the mean corotation radius, $\langle r_{\rm cor}/R_{25}\rangle \approx 0.45 \pm 0.03$. We will discuss these results below merging them with appropriate results obtained for GD and NGD subsamples.

We now investigate the existence of the possible radial trends of d_2 distributions for SNe Ibc and II separately in GD and NGD galaxies. The Spearman's rank correlation P-values of the radial trends are presented in Cols. 9 and 13 of Table 9. The definition of Cols. 6, 7, 8 and 10, 11, 12 is similar to Cols. 2, 3 and 4, but represent the values in GD and NGD galaxies, respectively. Here, the small number statistics for SNe Ibc probably play a role. Having this in mind,

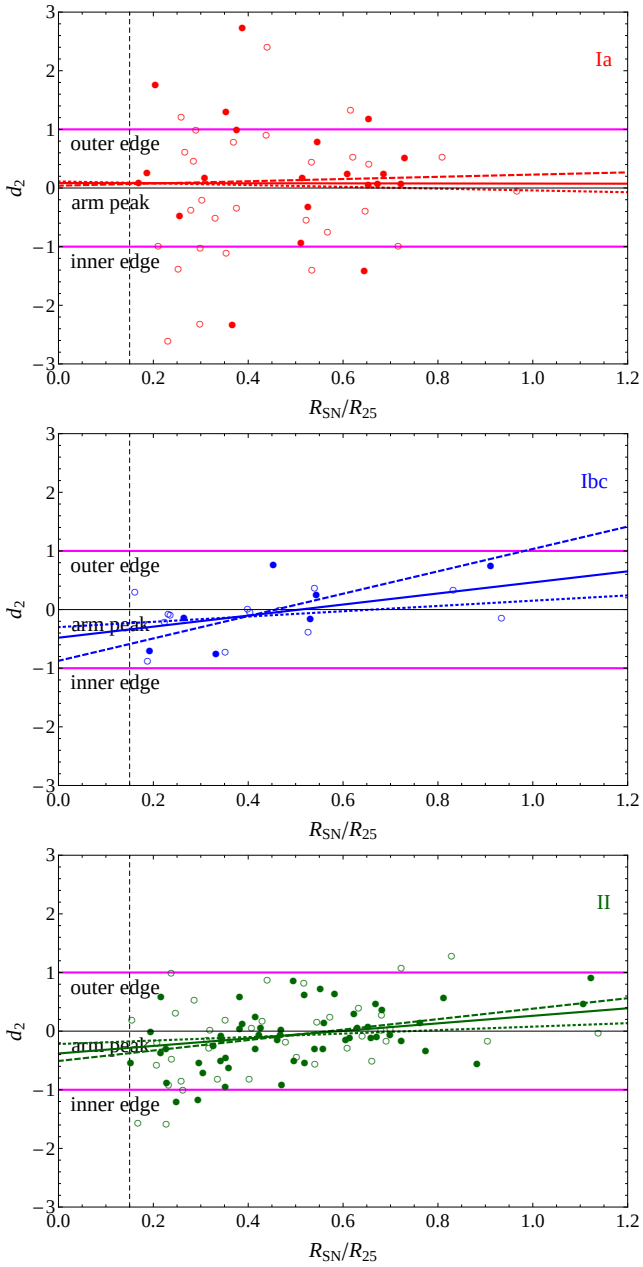

Figure 8. Distributions of the d_2 distances of SNe Ia (upper), Ibc (middle), and II (bottom) relative to the peaks of spiral arms versus the deprojected and normalized galactocentric distance. The data flagged by the "*" and ":" symbols are not considered. Filled and open circles respectively show SNe in GD and NGD galaxies. In all figures, the linear fits are given for the full (solid), GD (dashed), and NGD (dotted) samples. The inner and outer edges, as well the peaks of spiral arms are shown with parallel lines, similar to Fig. 2. The region to radius $R_{\rm SN}/R_{25} = 0.15$ (dashed vertical line) have been excluded from this analysis.

a positive significant correlation is observed in GD hosts for SNe II between d_2 and $R_{\rm SN}/R_{25}$. An even stronger correlation ($\rho = 0.57$) occurs for SNe Ibc, but it is not statistically significant probably due to the small number statistics (only 7 SNe Ibc in GD hosts). In contrast, in NGD galaxies we find no significant correlations between d_2 and $R_{\rm SN}/R_{25}$ for SNe Ibc and II.

Table 9. Spearman's rank correlation P-values of the radial trend of SNe distribution relative to the peaks of spiral arms. The statistically significant trends are highlighted in bold.

SNe	All spirals				GD galaxies				NGD galaxies			
	N_{SN}	a	ρ	P	N_{SN}	a	ρ	P	N_{SN}	a	ρ	P
(1)	(2)	(3)	(4)	(5)	(6)	(7)	(8)	(9)	(10)	(11)	(12)	(13)
Ia	34	-0.01 ± 0.72	0.013	0.942	15	0.19 ± 0.58	0.086	0.761	19	-0.15 ± 0.82	-0.096	0.694
Ibc	20	0.94 ± 0.39	0.465	**0.039**	7	1.91 ± 0.67	0.571	0.180	13	0.45 ± 0.41	0.302	0.316
II	87	0.64 ± 0.22	0.291	**0.006**	52	0.89 ± 0.27	0.385	**0.005**	35	0.30 ± 0.38	0.168	0.336

Similarly to the full sample of host galaxies, we split the CC SNe sample into two radial bins using the demarcation radius of $\langle r_{cor}/R_{25} \rangle$, for SNe in both GD and NGD host galaxies, and compare the distributions of their d_2 parameters. The results of KS and AD tests for GD and NGD hosts are $P_{KS} = 0.082$ ($P_{AD} = 0.024$) and $P_{KS} = 0.496$ ($P_{AD} = 0.281$), respectively. This means that, in contrast to NGD galaxies, the density waves of GD galaxies can strongly act on the star formation processes, thus exhibiting significant differences between distributions of CC SNe relative to peaks of spiral arms inside and outside the corotation radius. Most probably, the absence of such a distribution in the younger stellar component of NGD galaxies is due to the weaker nature of the density waves in NGD spirals.

In contrast to CC SNe, Fig. 8 and Table 9 show that the distribution of SNe Ia in spiral arms does not depend on the galactocentric radius in the full sample, as well as in both GD and NGD galaxies separately. Similar to CC SNe, we split the SNe Ia sample into two radial bins with the demarcation radius and compare the d_2 distributions of these SNe inside inner and outer radial bins. The differences between the two distributions in the full ($P_{KS} = 0.882$ and $P_{KS} = 0.720$), GD ($P_{KS} = 0.919$ and $P_{AD} = 0.722$) and NGD ($P_{KS} = 0.904$ and $P_{AD} = 0.815$) samples are not significant. It is important to note that the number of interarm SNe Ia is enhanced at smaller radii (see Fig. 8), which is probably due to the contribution of the old bulge component. However, we do not exclude that a significant part of these interarm SNe Ia belong to the disc population (Paper III).

5 DISCUSSION

The results described above deserve a deeper analysis in order to fully understand all the possible implications in the context of the host galaxy spiral structure and SN progenitor scenario.

Although the difference between the distributions of d_2 distances of the locations of SNe relative to the peak of spiral arms, normalized to the inner/outer semi-widths) of CC SNe in GD and NGD galaxies is not statistically significant (Sect. 4.2), the radial dependence of these distributions in GD and NGD galaxies have different behaviors (Sect. 4.3). In particular, in GD galaxies, a positive significant correlation exists between the galactocentric radius of SNe II and d_2, and an even stronger (but not significant) correlation occurs for SNe Ibc. In contrast, in NGD galaxies there are no significant correlations between these parameters. Since the progenitors of SNe Ibc and II belong to young stellar populations, we interpret the differences as the consequence of star formation processes in spiral arms and their differences between GD and NGD galaxies.

In NGD galaxies, the spiral arms are believed to originate from the shear of HII regions due to the differential rotation of the discs (e.g. Seiden & Gerola 1982; Elmegreen et al. 2003; Dobbs, Burkert & Pringle 2011). In contrast to GD galaxies, their spiral arms corotate with the discs and do not show signs of shocks in their leading edges (see review by Dobbs & Baba 2014). Therefore, one does not expect young stars to be concentrated towards one of the edges of arms in NGD galaxies. This scenario also predicts the absence of radial trends for the distributions of SNe Ibc and II inside the spiral arms. In NGD galaxies, we found that CC SNe are more concentrated towards the peaks of spiral arms than SNe Ia. Moreover, despite small number statistics, in NGD galaxies we found different concentration levels for SNe Ibc and II. In particular the mean absolute d_2 distance of SNe Ibc is 0.27 ± 0.08 ($N = 13$) and for SNe II is 0.49 ± 0.07 ($N = 39$). An AD test shows that the difference between the distributions of absolute distances of SNe Ibc and II from the peaks of spiral arms is barely significant ($P_{AD} = 0.074$, while $P_{KS} = 0.207$). Hence, in NGD galaxies the shortest mean distance to the peak of spiral arm is for SNe Ibc. In addition, the distribution of any SN type inside the spiral arms in NGD galaxies does not show any significant radial trend.

Assuming that 1) the g-band profiles of spiral arms represent the distribution of young stars, and 2) the peaks of spiral arms of NGD galaxies are the most suitable sites of the star formation, we propose that when the concentration of a given type of SNe towards the arm peak is higher, their progenitors are younger (more massive in the context of single-star evolution). Thus, a mass sequence Ia–II–Ibc for the SN progenitors is expected, in agreement with those from the literature obtained by the association of various SN types with the Hα emission of the host galaxy (e.g. James & Anderson 2006; Anderson & James 2008; Anderson et al. 2012). This also confirms the result of Kelly, Kirshner & Pahre (2008) for the local environment of the SNe, that SNe Ibc prefer to lie in relatively bright regions, in comparison with SNe II and Ia.

The distribution of SNe inside the spiral arms of GD galaxies is quiet different. In particular, in GD galaxies we found a significant shift between the distributions of distances of CC and Ia SNe from the peaks of spiral arms. In order to understand the possible effect of density waves on the observed offset, we pay attention to the fig. 4 of del Rio & Cepa (1998), representing the effect of a strong

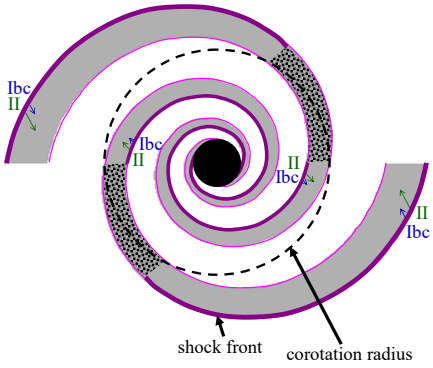

Figure 9. The scheme of star formation distribution in a model of two armed GD galaxy with the directions and relative sizes of drifts from birth places up to the explosion for SNe Ibc (blue arrow) and II (green arrow). For better visualization, the directions of drifts are shown with a significant radial component.

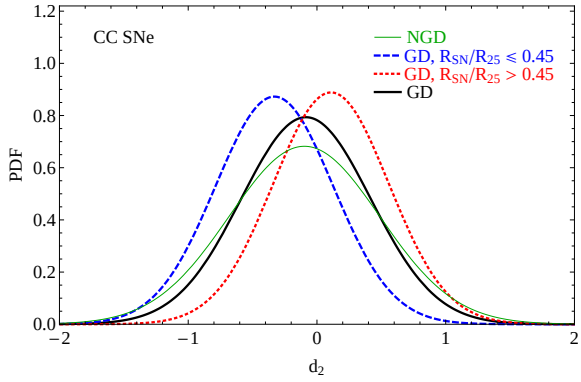

Figure 10. The fitted Gaussian functions of CC SNe distributions in NGD (thin green), GD (thick black), as well in inner ($R_{\rm SN}/R_{25} \leqslant 0.45$, dashed blue) and outer ($R_{\rm SN}/R_{25} > 0.45$, dotted red) galactocentric distances of GD galaxies.

density wave on the B- and I-band profiles of spiral arms before corotation radius. This figure shows that the strong density waves that cause the young stars to concentrate in the inner (leading) edges of spiral arms, lead to an intensity (brightness) profile that is skewed to the inner regions of spiral arms in the short wavebands (B and g) in comparison to the longer ones (I, e.g. del Rio & Cepa 1998; Martínez-García, González-López lira & Bruzual-A 2009). This effect is schematically illustrated in fig. 1 of Martínez-García et al. (2009). It is probably also reflected on the corresponding distributions of CC SNe versus SNe Ia in the upper panel of Fig. 7.

In addition, we found an offset (though non-significant) between the distributions of distances of SNe Ibc and II from the inner edges of the spiral arms. The observed offset between all types of SNe is ordered with the following sequence from inner edges Ibc-II-Ia (as in NGD galaxies). It is important to note that in GD hosts, there is a statistically significant positive correlation for *arm* SNe II between d_2 and $R_{\rm SN}/R_{25}$. The same correlation is found for SNe Ibc, with an even higher slope, but not significant because of small number statistics. The positions of both types of SNe beyond $R_{\rm SN}/R_{25} \approx 0.45$ (roughly the mean corotation radius) are now typically outside the peaks of the arms through the radius vector, while at smaller radii the positions of SNe are typically inside the peaks of the arms. Similar trends for star-forming regions are observed in some GD galaxies (e.g. Cedrés et al. 2013).

Adopting an average corotation radius of 0.45 R_{25}, the mean distances (d_1 inside and $1 - d_1$ outside the corotation radius, respectively) of SNe Ibc and II from leading edges of spiral arms are 0.25 ± 0.07 and 0.44 ± 0.03, respectively. KS and AD tests show that the difference between the distributions of SNe Ibc and II relative to leading edges of spiral arms is statistically significant ($P_{\rm KS} = 0.026$ and $P_{\rm AD} = 0.011$). According to the dynamical simulations by Dobbs & Pringle (2010), the observed concentration sequence towards the leading edges of spiral arms indicates a lifetime sequence (see the top-left panel of fig. 4 in Dobbs & Pringle 2010) for their progenitors (from youngest to oldest). Therefore, one may gain information about the lifetimes of SN progenitors from the amplitude of the shift and the adoption of an average corotation radius (the greater the mean distance from the leading edge, the longer is the progenitor's lifetime). It is important to note that the real migration of stars from their birthplace in the spiral arms is quite complex (e.g. Kubryk, Prantzos & Athanassoula 2013; Halle et al. 2015) and a detailed analysis of it is beyond the aim of this paper that tackles the issue just qualitatively.

The scheme of star formation in a model of a GD galaxy with two spiral arms with the directions and relative sizes of drifts from birth places up to the explosion for various SNe is given in the Fig. 9. Inside the corotation radius (dashed circle), star formation processes generally occur in a shock front at the inner (leading) edges of spiral arms. Since the disc rotates faster than the spiral arms inside the corotation radius, newborn stars near inner edges move towards the outer edges of spiral arms. On the contrary, outside the corotation radius, stars are caught up by the spiral arms, hence move from the outer edges of the arms towards the inner edges of spiral arms. In the corotation zone, there are no triggering mechanisms of star formation, such as spiral shocks. The main mechanism of star formation in this region (dotted surface of arms) is gravitation instability (as in NGD galaxies). Therefore, in this region, the distribution of SNe inside the spiral arms should have the same behavior as in NGD galaxies. Moreover, because of the absence of spiral shocks in this region, star formation (e.g. Elmegreen, Elmegreen & Montenegro 1992), hence the number of CC SNe, should exhibit a drop. Since more massive stars live shorter than less massive ones, their explosion sites are, on average, closer to the leading edges of arms where they born. The observed significantly shorter distances of SNe Ibc from the leading edges of spiral arms show that their progenitors are younger (more massive) than those of SNe II. This result is in agreement with the single-star progenitor scenario of SNe Ibc.

Since we cannot directly measure the corotation radii, using instead isophotal radii to scale our host galaxies, any dispersion of the corotation-to-isophotal radius ratio will blur the expected radial drop near corotation (see the continuous distribution in CC SN positions within arms versus galactocentric radius in Fig. 8). Nevertheless, the observed intersection of the linear fits to the normalized locations of CC SNe within arms (in units of isophotal radii) with the peaks of arms at precisely the typical corotation radii (again in units of isophotal radii) supports our conclusion that the locations of SNe are a combination of the circular velocity of stars in the disc relative to the pattern speed of the spiral arms and the ages of the progenitors.[11]

Our results show that to constrain the nature of CC SN progenitors, it is very important to take into account the spiral arm classes of host galaxies, as well the locations of SNe relative to the spiral arms of their host galaxies. We illustrate this in Fig. 10, where we show the best-fit Gaussians to the CC SNe distributions in NGD and GD galaxies, as well the distributions in inner ($R_{\rm SN}/R_{25} \leqslant 0.45$) and outer ($R_{\rm SN}/R_{25} > 0.45$) galactocentric distances. Fig. 10 shows that the distribution of distances of CC SNe relative to the peaks of spiral arms in NGD and GD (without radial separation) galaxies are similar, repeating our finding of Sect. 4.2 that the differences of these distributions are not statistically significant. However, when we separate the distribution in GD galaxies into two radial bins, they exhibit an obvious offset between each other, as well from the peaks of spiral arms, as we previously found in Sect. 4.3. The difference of the distributions of CC SNe in inner and outer radial bins of NGD galaxies is not statistically significant (Sect. 4.3). This shows that the distributions of d_1 and d_2 distances of SNe Ibc and II in the whole sample of host galaxies are the combinations of 3 different distributions: the one in NGD galaxies; the distribution at smaller ($R_{\rm SN}/R_{25} \leqslant 0.45$) and larger ($R_{\rm SN}/R_{25} > 0.45$) galactocentric distances of GD galaxies. Therefore, their combined distributions are less informative for the ages of SN progenitors. It is important to note that the previous studies (e.g. Bartunov et al. 1994; Mikhailova et al. 2007) suffer from this effect, and the obtained mean distances of SNe from the arm peaks in joint samples of host galaxies (GD+NGD) do not represent the mean distances from the birth places of SNe.

We stress that the d_2 distribution of SNe Ia relative to spiral arms of GD and NGD galaxies exhibits a similar behavior. In both types of galaxies, these distributions are significantly different from the distributions of CC SNe. In addition, in both samples of galaxies these distributions do not show any significant dependence on galactocentric distances. This means that the progenitors of SNe Ia arise from a population that is old enough to migrate away (in both radial and azimuthal directions) from their birth places during their lifetimes, thus representing only the distribution of the older stellar population.

[11] The distribution of SNe relative to the estimated corotation radii will be investigated in our forthcoming paper, with about twice larger sample and without restrictions on the environments of SNe in galaxies.

6 CONCLUSIONS

In this fourth paper of our series of articles on the relation between SNe and their host galaxies, we analyse the distributions of different types of SNe relative to spiral arms of galaxies with different arm classes. We use a large and homogeneous sample to study the nature of SN progenitors, through the star formation processes in spiral galaxies and their possible triggering mechanisms. The sample of this analysis consists of 187 spiral galaxies, which host 215 SNe in total. Out of these 215 SNe, 106 occurred in GD galaxies and 109 in NGD galaxies.

The main results of the article and their interpretations are summarized below.

(i) The most significant parameter for a quantitative analysis of the spatial distribution of SNe inside the spiral arms is d_2 (the distance of an SN from the peak of its spiral arm, normalized to the inner/outer semi-width), as defined in Sect. 3.3 (eq. [2]).

(ii) For all SNe, the distribution of d_2 values is in agreement with a Gaussian, centred on zero (corresponding to the peak of the arm). However, SNe Ibc are most concentrated around the arm peaks, SNe II less so, while SNe Ia display the weakest concentration around the peaks.

(iii) The distributions of SNe Ia and CC SNe relative to peaks of spiral arms are significantly different from each other in both GD and NGD galaxies. Moreover, the peaks of the distributions of Type Ia and CC SNe in GD galaxies show offsets similar to the color gradients in spiral arms, as predicted from density wave theory (e.g. del Rio & Cepa 1998; Martínez-García et al. 2009).

(iv) In NGD hosts, no significant correlation is observed between d_2 and $R_{\rm SN}/R_{25}$ for *arm* SNe Ibc and II. This is probably due to the nature of spiral arms of NGD galaxies, that reflects the distribution of massive star formation in arms of these hosts.

(v) In GD hosts, a statistically significant positive correlation is observed between d_2 and $R_{\rm SN}/R_{25}$ for *arm* SNe II. An even stronger correlation is present for SNe Ibc, but is not statistically significant, due to their small number statistics. Most probably, because of the shorter lifetimes of their progenitors, the slope of the radial trend of SNe Ibc is higher than that for SNe II.

(vi) In GD galaxies, the distribution of d_2 distances of CC SNe in two different radial bins (with demarcation radius $r_{\rm cor}/R_{25} \approx 0.45$) are significantly different, while in NGD the difference is not significant.

(vii) A similar comparison of the distributions of d_2 of SNe Ia with the same demarcation radius ($r_{\rm cor}/R_{25} \approx 0.45$) in both GD and NGD galaxies shows no significant differences. Moreover, for SNe Ia, d_2 shows no significant dependence on $R_{\rm SN}/R_{25}$.

(viii) In GD galaxies, the distributions of distances of SNe Ibc and II from the leading edges are significantly different. SNe Ibc occur at smaller distances from the leading edges of arms than that of SNe II. Hence, the d_2 versus $R_{\rm SN}/R_{25}$ correlation for SNe Ibc and II in GD galaxies is in agreement with the density wave-induced star formation model and with the following lifetime sequence of SN progenitors: Ibc-II-Ia.

The results of this study show that the distribution of

SNe relative to spiral arms is a powerful tool to constrain the lifetimes (masses) of their progenitors and to better understand the star formation processes in various types of spiral galaxies.

ACKNOWLEDGMENTS

We would like to thank the referee, Phil James, for constructive comments that improved the clarity of this paper. LSA, AAH, and ARP acknowledge the hospitality of the Institut d'Astrophysique de Paris (France) during their stay as visiting scientists supported by the Collaborative Bilateral Research Project of the State Committee of Science (SCS) of the Republic of Armenia and the French Centre National de la Recherché Scientifique (CNRS). This work was supported by State Committee Science MES RA, in frame of the research project number SCS 13–1C013. AAH is also partially supported by the ICTP. VA is supported by grant SFRH/BPD/70574/2010 from FCT (Portugal). DK acknowledges financial support from the Centre National d'Études Spatiales (CNES). MT is partially supported by the PRIN-INAF 2011 with the project Transient Universe: from ESO Large to PESSTO. This work was made possible in part by a research grant from the Armenian National Science and Education Fund (ANSEF) based in New York, USA. Funding for SDSS-III has been provided by the Alfred P. Sloan Foundation, the Participating Institutions, the National Science Foundation, and the US Department of Energy Office of Science. The SDSS–III web site is `http://www.sdss3.org/`. SDSS–III is managed by the Astrophysical Research Consortium for the Participating Institutions of the SDSS–III Collaboration including the University of Arizona, the Brazilian Participation Group, Brookhaven National Laboratory, University of Cambridge, University of Florida, the French Participation Group, the German Participation Group, the Instituto de Astrofisica de Canarias, the Michigan State/Notre Dame/JINA Participation Group, Johns Hopkins University, Lawrence Berkeley National Laboratory, Max Planck Institute for Astrophysics, New Mexico State University, New York University, Ohio State University, Pennsylvania State University, University of Portsmouth, Princeton University, the Spanish Participation Group, University of Tokyo, University of Utah, Vanderbilt University, University of Virginia, University of Washington, and Yale University.

REFERENCES

Anderson J. P., James P. A., 2008, MNRAS, 390, 1527
Anderson J. P., James P. A., 2009, MNRAS, 399, 559
Anderson J. P., Habergham S. M., James P. A., Hamuy M., 2012, MNRAS, 424, 1372
Anderson J. P., James P. A., Förster F., González-Gaitán S., Habergham S. M., Hamuy M., Lyman J. D., 2015, MNRAS, 448, 732
Ann H. B., Lee H.-R., 2013, Journal of Korean Astronomical Society, 46, 141
Aramyan L. S., Petrosian A. R., Hakobyan A. A., Mamon G. A., Kunth D., Turatto M., Adibekyan V. Z., Nazaryan T. A., 2013, Astrophysics, 56, 153
Bartunov O. S., Tsvetkov D. Y., Filimonova I. V., 1994, PASP, 106, 1276
Bertin E., Arnouts S., 1996, A&AS, 117, 393
Bertin G., Lin C. C., Lowe S. A., Thurstans R. P., 1989, ApJ, 338, 78
Boissier S., Prantzos N., 2009, A&A, 503, 137
Buta R. J., 2013, Galaxy Morphology. p. 1, doi:10.1007/978-94-007-5609-0˙1
Cameron E., 2011, PASA, 28, 128
Cappellaro E., Evans R., Turatto M., 1999, A&A, 351, 459
Casteels K. R. V., et al., 2013, MNRAS, 429, 1051
Cedrés B., Cepa J., Bongiovanni Á., Castañeda H., Sánchez-Portal M., Tomita A., 2013, A&A, 560, A59
Crowther P. A., 2013, MNRAS, 428, 1927
Dobbs C., Baba J., 2014, PASA, 31, 35
Dobbs C. L., Pringle J. E., 2010, MNRAS, 409, 396
Dobbs C. L., Burkert A., Pringle J. E., 2011, MNRAS, 417, 1318
Elmegreen D. M., Elmegreen B. G., 1987, ApJ, 314, 3
Elmegreen B. G., Elmegreen D. M., 1989, ApJ, 342, 677
Elmegreen B. G., Elmegreen D. M., Montenegro L., 1992, ApJS, 79, 37
Elmegreen B. G., Elmegreen D. M., Leitner S. N., 2003, ApJ, 590, 271
Foyle K., Rix H.-W., Dobbs C. L., Leroy A. K., Walter F., 2011, ApJ, 735, 101
Garcia-Burillo S., Guelin M., Cernicharo J., 1993, A&A, 274, 123
Georgy C., Ekström S., Meynet G., Massey P., Levesque E. M., Hirschi R., Eggenberger P., Maeder A., 2012, A&A, 542, A29
Habergham S. M., James P. A., Anderson J. P., 2012, MNRAS, 424, 2841
Hakobyan A. A., Mamon G. A., Petrosian A. R., Kunth D., Turatto M., 2009, A&A, 508, 1259
Hakobyan A. A., et al., 2011, Astrophysics, 54, 301
Hakobyan A. A., Adibekyan V. Z., Aramyan L. S., Petrosian A. R., Gomes J. M., Mamon G. A., Kunth D., Turatto M., 2012, A&A, 544, A81 (Paper I)
Hakobyan A. A., et al., 2014, MNRAS, 444, 2428 (Paper II)
Hakobyan A. A., et al., 2016, MNRAS, 456, 2848 (Paper III)
Halle A., Di Matteo P., Haywood M., Combes F., 2015, A&A, 578, A58
James P. A., Anderson J. P., 2006, A&A, 453, 57
Kelly P. L., Kirshner R. P., 2012, ApJ, 759, 107
Kelly P. L., Kirshner R. P., Pahre M., 2008, ApJ, 687, 1201
Kendall S., Kennicutt R. C., Clarke C., 2011, MNRAS, 414, 538
Kormendy J., Norman C. A., 1979, ApJ, 233, 539
Kubryk M., Prantzos N., Athanassoula E., 2013, MNRAS, 436, 1479
Kuncarayakti H., et al., 2013a, AJ, 146, 30
Kuncarayakti H., et al., 2013b, AJ, 146, 31
Li W., Chornock R., Leaman J., Filippenko A. V., Poznanski D., Wang X., Ganeshalingam M., Mannucci F., 2011, MNRAS, 412, 1473
Mannucci F., Della Valle M., Panagia N., Cappellaro E., Cresci G., Maiolino R., Petrosian A., Turatto M., 2005, A&A, 433, 807
Maoz D., Mannucci F., 2012, PASA, 29, 447
Martínez-García E. E., González-López lira R. A., Bruzual-A G., 2009, ApJ, 694, 512
Maza J., van den Bergh S., 1976, ApJ, 204, 519
McMillan R. J., Ciardullo R., 1996, ApJ, 473, 707
Mikhailova G. A., Bartunov O. S., Tsvetkov D. Y., 2007, Astronomy Letters, 33, 715
Moore E., 1973, PASP, 85, 564
Navasardyan H., Petrosian A. R., Turatto M., Cappellaro E., Boulesteix J., 2001, MNRAS, 328, 1181
Nazaryan T. A., Petrosian A. R., Hakobyan A. A., Adibekyan V. Z., Kunth D., Mamon G. A., Turatto M., Aramyan L. S., 2013, Ap&SS, 347, 365
Petrosian A., et al., 2005, AJ, 129, 1369
Roberts W. W., 1969, ApJ, 158, 123

Sánchez-Gil M. C., Jones D. H., Pérez E., Bland-Hawthorn J., Alfaro E. J., O'Byrne J., 2011, MNRAS, 415, 753
Sanders R. H., Huntley J. M., 1976, ApJ, 209, 53
Scarano S., Lépine J. R. D., 2013, MNRAS, 428, 625
Seiden P. E., Gerola H., 1982, Fund. Cosmic Phys., 7, 241
Seigar M. S., James P. A., 2002, MNRAS, 337, 1113
Sellwood J. A., 2013, Dynamics of Disks and Warps. p. 923, doi:10.1007/978-94-007-5612-0˙18
Smartt S. J., 2009, ARA&A, 47, 63
Spergel D. N., et al., 2007, ApJS, 170, 377
Tamburro D., Rix H.-W., Walter F., Brinks E., de Blok W. J. G., Kennicutt R. C., Mac Low M.-M., 2008, AJ, 136, 2872
Toomre A., Toomre J., 1972, ApJ, 178, 623
Tsvetkov D. Y., Blinnikov S. I., Pavlyuk N. N., 2001, Astronomy Letters, 27, 411
Vogel S. N., Kulkarni S. R., Scoville N. Z., 1988, Nature, 334, 402
Zhang X., 1996, ApJ, 457, 125
Zhang X., 1998, ApJ, 499, 93
Zhang X., 1999, ApJ, 518, 613
del Rio M. S., Cepa J., 1998, A&A, 340, 1
van Dyk S. D., Hamuy M., Filippenko A. V., 1996, AJ, 111, 2017
van den Bergh S., 1997, AJ, 113, 197

APPENDIX A: SN AND HOST GALAXY DATA

Table A1. List of *arm* SNe.

SN (1)	Type[a] (2)	Galaxy (3)	Morph.[a] (4)	Arm Class (5)	R_{SN}/R_{25} (6)	d_1^b (7)	d_2^b (8)
1921B	II	NGC 3184	Sc	NGD	0.74	0.65:	0.30:
1937F	II P:	NGC 3184	Sc	NGD	0.68	0.43	0.03
1947A	II	NGC 3177	Sb	NGD	0.97	0.67	···
1951H	II:	NGC 5457	Sc	GD	0.52	0.75	0.62
1961U	II L	NGC 3938	Sc	GD	0.76	0.49	0.15
1963J	Ia	NGC 3913	Sc	GD	0.17	0.44	0.09
1964A	II pec	NGC 3631	Sc	GD	1.12	0.95	0.91
1964L	Ic	NGC 3938	Sc	GD	0.19	0.16	–0.70
1965L	II P	NGC 3631	Sc	GD	0.67	0.58	–0.10
1966K	Ia:	MCG +05–27–53	Sab	GD	0.72	0.50	0.08
1967H	II:	NGC 4254	Sc	GD	0.47	0.39	0.02
1970G	II L	NGC 5457	Sc	GD	0.55	0.83	0.73
1972Q	II P	NGC 4254	Sc	GD	0.66	0.36	–0.11
1973U	II	IC 43	SBc	NGD	0.57	0.57	0.25
1974J	Ia*	NGC 7343	SBb	NGD	0.57	0.05	–0.73
1975O	Ia*	NGC 2487	SBc	GD	0.45	0.49*	–0.02*
1978B	II	MCG +10–16–117	Sd	GD	0.56	0.43	–0.29
1978H	II	NGC 3780	Sc	NGD	0.24	0.25	–0.46
1979C	II L	NGC 4321	Sc	GD	0.58	0.77	0.65
1983I	Ib/c	NGC 4051	SBbc	NGD	0.40	0.25	0.02
1986A	Ia	NGC 3367	SBc	NGD	0.29	0.63	0.46
1986I	II P	NGC 4254	Sc	GD	0.23	0.29	–0.29
1987B	IIn L	NGC 5850	SBb	GD	1.11	0.73	0.47
1988O	Ia	PGC 0054128	Sc	NGD	0.37	0.89	0.79
1988R	Ia	MCG +09–23–09	Sc	NGD	0.38	0.27*	–0.47*
1989K	II	NGC 5375	SBbc	NGD	0.68	0.66	0.29
1990ag	II pec	A073249+3254	Sc	GD	0.34	0.48*	–0.04*
1991S	Ia	UGC 5691	Sbc	GD	0.65	0.44	0.06
1992C	II	NGC 3367	SBc	NGD	0.48	0.51*	0.02*
1992aa	IIn	NGC 6464	SBc	GD	0.61	0.46	–0.11
1992ad	II	NGC 4411B	Scd	NGD	0.50	0.22	–0.42
1992am	II P	PGC 0005247	SBb	GD	0.81	0.75	0.57
1993Z	Ia	NGC 2775	Sa	NGD	0.30	0.26	–0.19
1993ab	Ia	NGC 1164	SBab	GD	0.51	0.38	0.17
1994A	II	UGC 8214	SBb	GD	0.35	0.02	–0.95
1994K	Ia	PGC 0028944	SBbc	NGD	0.81	0.77	0.54
1995G	IIn	NGC 1643	SBbc:	GD	0.50	0.19	–0.51
1995Z	II	UGC 937	SBd	NGD	0.44	0.92	0.88
1996an	II	NGC 1084	Sc	NGD	0.23	0.56*	0.12*
1996cd	Ib/c:	A075720+1112	SBbc	NGD	0.53	0.25	–0.37
1997ef	Ic pec	UGC 4107	Sc	NGD	0.49	0.91*	0.83*
1997ei	Ic	NGC 3963	SBbc	GD	0.18	0.37*	–0.25*
1998C	II	UGC 3825	SBc	NGD	0.35	0.02:	–0.95:
1998V	Ia	NGC 6627	SBb	GD	0.53	0.46	–0.31
1998ab	Ia pec	NGC 4704	SBbc	NGD	0.47	0.16*	–0.67*
1998aq	Ia	NGC 3982	Sbc	NGD	0.33	0.25	–0.5
1998dl	II	NGC 1084	Sc	NGD	0.24	1.00	1.00
1999K	II	A080306+0324	SBd	GD	0.67	0.21	···
1999bg	II:	IC 758	SBd	GD	0.61	0.43	–0.14
1999br	II pec	NGC 4900	SBd	NGD	0.57	0.79	···
1999di	Ib	NGC 776	Sbc	GD	0.36	0.19:	–0.62:
1999dk	Ia	UGC 1087	Sc	NGD	0.65	0.71	0.41
1999do	Ia	MCG +05–54–03	Sa:	NGD	0.21	0.02	–0.97
1999ef	Ia	UGC 607	SBc	GD	0.69	0.64	0.25
1999et	II	NGC 1643	SBbc:	GD	0.34	0.42	–0.07
1999gb	IIn	NGC 2532	Scd	NGD	0.31	0.51:	0.03:
1999ge	II	NGC 309	SBc	GD	0.19	0.38	–0.01
1999gi	II P	NGC 3184	Sc	NGD	0.28	0.70:	0.41:
1999gk	II	NGC 4653	Scd	NGD	0.61	0.55	–0.28
1999gn	II	NGC 4303	SBbc	GD	0.24	0.41*	–0.19*
2000F	Ic:	IC 302	SBbc	NGD	0.31	0.11	···
2000J	II	UGC 8510	SBc	GD	0.82	0.09	···
2000O	Ia	MCG +03–31–61	SBd	GD	0.67	0.44	0.08

Table A1. *Continued...*

SN (1)	Type[a] (2)	Galaxy (3)	Morph.[a] (4)	Arm Class (5)	R_{SN}/R_{25} (6)	d_1^b (7)	d_2^b (8)
2000cq	II	UGC 10354	Scd	GD	0.88	0.29	–0.55
2000ct	IIn	A170103+3328	SBd	NGD	0.66	0.72	···
2000dq	II	MCG +00–06–43	Sbc	GD	0.55	0.09*	–0.82*
2000du	II	UGC 3920	Sb	GD	0.42	0.60	0.24
2001J	II	UGC 4729	SBd	NGD	0.55	0.78	0.17
2001Q	II	UGC 6429	Sc	GD	0.42	0.53	–0.06
2001Y	II pec	NGC 3362	Sc	GD	0.46	0.50	–0.14
2001aj	II	UGC 10243	Sc	NGD	0.52	0.91	0.84
2001fv	II	NGC 3512	Sc	NGD	0.54	0.27:	–0.47:
2001it	II	MCG +09–25–15	Sc	GD	0.33	0.29	–0.24
2002ap	Ic pec	NGC 628	Sc	GD	0.91	0.88	0.75
2002at	II:	NGC 3720	Sb	NGD	0.22	0.50*	0.00*
2002ca	II	UGC 8521	SBab	NGD	0.41	0.97:	0.94:
2002cb	IIn	MCG +08–24–34	SBc	GD	0.56	0.43	0.14
2002cp	Ib/c	NGC 3074	Scd	NGD	0.93	0.64	–0.14
2002df	Ia	MCG –01–53–06	SBc	NGD	0.72	0.02	–0.97
2002en	II	UGC 12289	SBc	GD	0.41	0.28	–0.30
2002fj	IIn	NGC 2642	SBbc	GD	0.32	0.44:	–0.12:
2002ji	Ib/c	NGC 3655	Sbc	NGD	0.35	0.14	–0.72
2003C	II	UGC 439	Sb	GD	0.22	0.69	0.59
2003G	IIn	IC 208	Sc	NGD	0.23	0.05	–0.90
2003L	Ic	NGC 3506	Sc	NGD	0.23	0.36	–0.06
2003T	II	UGC 4864	Sb	GD	0.52	0.25	–0.54
2003cq	Ia	NGC 3978	Sc	NGD	0.52	0.25	–0.54
2003ej	II	UGC 7820	Scd	NGD	0.64	0.53	–0.07
2003el	Ic	NGC 5000	SBbc	GD	0.32	0.51:	0.01:
2003fd	Ia	UGC 8670	SBcd	GD	0.61	0.55	0.25
2003gd	II P	NGC 628	Sc	GD	0.62	0.64	0.30
2003hq	Ia	MCG +08–30–27	SBbc	GD	0.38	1.00	1.00
2003ih	Ib/c	UGC 2836	Sa	NGD	0.16	0.77	0.31
2003iy	II:	NGC 6143	Sc	NGD	0.21	0.13	–0.57
2003kw	II	UGC 6314	SBbc	GD	0.30	0.31	–0.53
2004K	Ia	E579–G22	SBb	GD	0.51	0.03	–0.94
2004T	II	UGC 6038	Sb	GD	0.38	0.55	0.05
2004bk	Ia	NGC 5246	SBb	GD	0.36	0.48*	–0.03*
2004ef	Ia	UGC 12158	SBbc	GD	0.26	0.27	–0.47
2004er	II	MCG –01–07–24	Scd	NGD	0.63	0.71	0.41
2004es	II	UGC 3825	SBc	NGD	0.69	0.50	–0.16
2004ey	Ia	UGC 11816	SBc	NGD	0.28	0.27	–0.36
2004gx	II:	UGC 12663	SBc	NGD	0.29	0.69	0.54
2005I	II	IC 983	SBbc	NGD	0.35	0.69	0.19
2005ao	Ia	NGC 6462	Sb	NGD	0.65	0.33	–0.38
2005ay	II P	NGC 3938	Sc	GD	0.35	0.16	–0.45
2005bh	Ic	UGC 6495	SBc	GD	0.53	0.40	–0.15
2005bj	Ic:	MCG +03–43–05	SBd	NGD	0.47	0.63	0.00
2005bk	Ic	MCG +07–33–27	Sab	NGD	0.19	0.06	–0.86
2005cl	IIn	MCG –01–53–20	SBb	GD	0.47	0.02	–0.91
2005cv	II	UGC 1359	Sb	GD	0.22	0.19	–0.36
2005dz	II	UGC 12717	Sc	NGD	0.66	0.26	–0.49
2005es	II	MCG +01–59–79	Sbc	GD	0.34	0.25	–0.14
2005gl	IIn	NGC 266	SBb	GD	0.28	0.46:	–0.07:
2005gm	II	NGC 1423	SBb	GD	0.43	0.44	0.06
2005lt	Ia	MCG +03–30–51	SBc	NGD	0.62	0.80	0.53
2006G	IIb	NGC 521	SBbc	GD	0.47	0.50	–0.06
2006ac	Ia	NGC 4619	SBbc	NGD	0.44	0.94	0.92
2006ad	II	A090743+1203	SBd	GD	0.81	0.50	···
2006bl	II	MCG +02–40–09	Sc	NGD	0.32	0.50	0.03
2006cp	Ia	UGC 7357	SBd	NGD	0.53	0.69	0.46
2006cy	IIn	A130801+2606	Sc	NGD	0.54	0.30	–0.54
2006dl	IIb	MCG +04–31–05	Sc:	NGD	0.40	0.07	–0.81
2006dp	II	MCG –01–03–56	Sbc	GD	0.23	0.06	–0.88
2006en	Ia	MCG +05–54–41	Sbc:	NGD	0.19	0.11*	–0.79*
2006es	Ia	UGC 2828	SBbc	GD	0.28	0.83:	0.65:

Table A1. *Continued...*

SN (1)	Type[a] (2)	Galaxy (3)	Morph.[a] (4)	Arm Class (5)	R_{SN}/R_{25} (6)	d_1^b (7)	d_2^b (8)
2006gs	II	NGC 3977	Sc	NGD	0.21	0.45	–0.20
2006jd	IIn	UGC 4179	SBbc	NGD	0.57	0.44*	–0.13*
2007F	Ia	UGC 8162	SBc	GD	0.36	0.13	···
2007K	IIn	MCG +06–20–50	SBb	GD	0.30	0.17	–0.71
2007O	Ia	UGC 9612	SBc	GD	0.19	0.67	0.26
2007aa	II	NGC 4030	Sbc	GD	0.67	0.74	0.46
2007ad	II	UGC 10845	Sc	NGD	0.31	0.42	–0.15
2007am	II	NGC 3367	SBc	NGD	0.25	0.60	0.31
2007aq	II P	IC 2409	Sbc	NGD	0.90	0.53	–0.15
2007ay	IIb	UGC 4310	Scd	NGD	0.48	0.26	–0.17
2007bc	Ia	UGC 6332	Sab	GD	0.78	0.48	···
2007bp	II	A092400+0512	Sc	GD	0.36	0.18	–0.62
2007bv	II	A153410+0705	SBb	GD	0.39	0.34	0.13
2007cl	Ic	NGC 6479	Sc	GD	0.26	0.22	–0.14
2007gl	Ib/c	A031133–0044	Sbc	GD	0.54	0.62	0.26
2007hb	Ib/c	NGC 819	Sbc	GD	0.45	0.84	0.77
2007il	II	IC 1704	Sc	NGD	0.43	0.59	0.19
2007pk	IIn pec	NGC 579	Scd	NGD	0.15	0.59	0.20
2007rt	IIn	UGC 6109	Sc	GD	0.15	0.23	–0.53
2008ae	Ia pec	IC 577	Sbc	GD	0.55	0.88	0.80
2008bh	II	NGC 2642	SBbc	GD	0.38	0.74	0.58
2008bl	II	UGC 9317	SBcd	NGD	0.32	0.35	–0.28
2008bs	Ib	UGC 4085	Sc	NGD	0.22	0.33	–0.20
2008cx	IIb	NGC 309	SBc	GD	0.63	0.65	0.07
2008du	Ic	NGC 7422	SBb	NGD	0.24	0.45	–0.08
2008dz	II	NGC 5123	Sc	GD	0.68	0.65	0.37
2008ew	Ic	IC 1236	SBc	GD	0.33	0.11	–0.75
2008ie	IIb	NGC 1070	Sc	NGD	0.26	0.00	–1.00
2008in	II P	NGC 4303	SBbc	GD	0.50	0.92	0.87
2009W	II P	A162347+1144	SBb	NGD	1.14	0.42	–0.03
2009af	II	UGC 1551	SBd	NGD	0.26	0.06	–0.84
2009ay	II	NGC 6479	Sc	GD	0.34	0.23*	–0.54*
2009bv	Ia	MCG +06–29–39	Sc	GD	0.73	0.73	0.51
2009cz	Ia	NGC 2789	Sa	NGD	0.38	0.20	–0.33
2009en	Ia	UGC 9515	SBc	NGD	0.57	0.12:	–0.76:
2009gk	IIb	UGC 11803	Sbc	NGD	0.70	0.34	0.05
2009ha	Ib	MCG –01–07–24	Scd	NGD	0.40	0.43	–0.03
2009ik	Ia	NGC 4653	Scd	NGD	0.97	0.67	–0.05
2009ls	II	NGC 3423	Scd	NGD	0.34	0.15	–0.81
2009lx	II P	MCG +01–30–08	SBb	GD	0.77	0.34	–0.33
2010av	Ib/c:	IC 1099	SBc	NGD	0.54	0.69	0.39
2010bs	II	UGC 7416	SBb	GD	0.70	0.55	–0.07
2010ct	II P:	NGC 3362	Sc	GD	0.72	0.44	–0.17
2010fz	Ia	NGC 2967	Sc	NGD	0.27	0.83	0.63
2010gs	II	MCG –01–53–07	Sbc	GD	0.65	0.52	0.08
2010ig	Ib	UGC 1306	SBa	NGD	0.83	0.53	0.34
2010jc	II P	NGC 1033	Sc	NGD	0.90	0.23	···
2011ak	II P	UGC 6997	Sd	GD	0.54	0.43	–0.29
2011an	IIn	UGC 4139	SBcd	NGD	0.41	0.52	0.06
2011bc	Ia	NGC 4076	Sbc	NGD	0.29	1.00	1.00
2011bi	II P	MCG +07–35–37	Sc	GD	0.34	0.33	–0.50
2011bk	Ia	A162034+2112	SBbc	GD	0.31	0.60	0.18

[a] Among all the SNe and host galaxy morphological types, there are some uncertain (':' or '?') and peculiar ('pec') classifications. In two cases, marked by '*', the Ia type has been inferred from the light curve only.

[b] The distance is flagged by a '*' or ':' symbol when one of the edges of the spiral arm is roughly determined. In these cases, the contaminated (by the light of a star or by the SN itself) edge is determined as a symmetric reflection of the other edge from the peak. The '*' symbol indicates that the SN is located between the peak and the roughly determined edge of the arm, while the ':' symbol indicates that the SN is located between the well-determined edge and the peak. In 10 cases, the d_2 parameter was not determined because of a noisy arm profile.

Table A2. List of *interarm* SNe.

SN (1)	Type[a] (2)	Galaxy (3)	Morph.[a] (4)	Arm Class (5)	R_{SN}/R_{25} (6)	d_1^b (7)	d_2^b (8)
1941C	II	NGC 4136	SBc	NGD	0.68	–0.37	···
1963D	Ia*	NGC 4146	SBb	GD	0.65	1.09	1.18
1963P	Ia	NGC 1084	Sc	NGD	0.26	1.12	1.23
1971U	Ia	MCG +05–26–14	SBcd	NGD	0.25	–0.22	–1.37
1978E	Ia	MCG +06–49–36	Sc	NGD	0.53	–0.19	–1.39
1979B	Ia	NGC 3913	Sc	GD	0.51	–0.03	···
1987C	IIn P	MCG +09–14–47	SBc	NGD	0.72	1.05	1.08
1989A	Ia	NGC 3687	SBc	NGD	0.44	1.71	2.41
1991am	Ia	MCG +06–37–06	Sb	NGD	0.30	–0.56	–2.30
1992ap	Ia	UGC 10430	SBbc	NGD	0.62	1.20	1.34
1997aa	II	IC 2102	SBd	NGD	0.85	–0.06	···
2001fa	IIn	NGC 673	Sc	GD	0.27	1.03	···
2001gb	Ia	IC 582	Sc	NGD	0.51	–0.15	···
2002hw	Ia	UGC 52	Sc	NGD	0.16	1.92	3.30
2003P	Ia	MCG +09–13–107	Sbc	NGD	0.23	–0.42	···
2003U	Ia	NGC 6365A	Sc	GD	0.35	1.17	1.30
2003ie	II	NGC 4051	SBbc	NGD	0.63	1.07	···
2004G	II	NGC 5668	Sd	NGD	0.41	–0.05	···
2004dv	II	MCG –01–06–12	SBcd	NGD	0.83	1.18	1.30
2005dq	II	UGC 12177	SBc	GD	0.20	–0.06	···
2005he	II	MCG +06–49–68	SBc	NGD	0.23	–0.29	–1.58
2005ms	Ia	UGC 4614	Scd	NGD	1.16	1.40	···
2006V	II	UGC 6510	SBcd	GD	0.77	–0.15	···
2006X	Ia	NGC 4321	Sc	GD	0.29	–0.11	···
2006dh	Ia	UGC 8670	SBcd	GD	0.39	1.79	2.74
2007kk	Ia	UGC 2828	SBbc	GD	0.37	–0.66	–2.32
2008dr	Ia	NGC 7222	SBbc	GD	0.23	–1.46	–3.9
2008el	II P	PGC 70567	Sbc	GD	1.00	1.17	···
2008fe	II P	UGC 9578	SBbc	NGD	0.75	–0.07	···
2008gi	II	A024400+0525	SBd	NGD	0.17	–0.15	–1.55
2009I	Ia	NGC 1080	Sc	NGD	0.35	–0.05	–1.10
2009ig	Ia	NGC 1015	SBa	NGD	0.30	–0.01	–1.02
2009iq	II P	UGC 2308	Sc	GD	0.25	–0.11	–1.21
2010B	Ia	NGC 5370	SBa	NGD	0.23	–0.41	–2.60
2010Z	II	NGC 2797	Sb	GD	0.29	–0.08	–1.12
2010hz	Ia	UGC 1359	Sb	GD	0.20	1.38	1.77
2010ii	Ia	NGC 7342	SBab	GD	0.64	–0.27	–1.41

The symbols used in this table are the same as in Table A1.